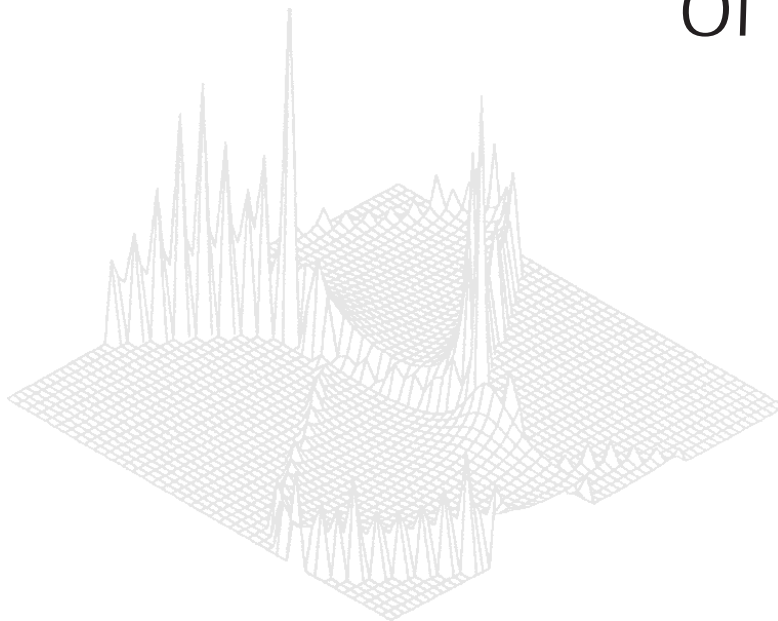

CSIRO PUBLISHING

Australian Journal of Physics

Volume 51, 1998
© CSIRO 1998



A journal for the publication of
original research in all branches of physics

www.publish.csiro.au/journals/ajp

All enquiries and manuscripts should be directed to

Australian Journal of Physics

CSIRO PUBLISHING

PO Box 1139 (150 Oxford St)

Collingwood

Vic. 3066

Australia

Telephone: 61 3 9662 7626

Facsimile: 61 3 9662 7611

Email: peter.robertson@publish.csiro.au



Published by **CSIRO PUBLISHING**
for CSIRO and the
Australian Academy of Science



Neutron Magnetic Tomography: A Feasibility Study*

H. Leeb,^A M. Hochhold, G. Badurek, R. J. Buchelt and A. Schrickner

Institut für Kernphysik, Technische Universität Wien,
Wiedner Hauptstrasse 8–10/142, A-1040 Vienna, Austria.

^ACorresponding author: leeb@kph.tuwien.ac.at.

Abstract

Neutron magnetic tomography, the recently proposed extension of the neutron depolarisation technique, is considered. The available numerical methods for the analysis of the data are reviewed and the possibility of visualising the magnetic structure within bulk materials is demonstrated by specific examples. Various ways to implement the method experimentally are presented. Estimates of the feasibility in terms of required measuring time indicate that visualisation is within experimental reach with modern neutron optical devices.

1. Introduction

The study of solid state systems by neutron physical techniques is well established. The vanishing charge and the finite magnetic moment of the neutron makes it a unique probe for the magnetic structure of materials. The possibility of investigating the magnetic domain structure of materials is offered by the neutron depolarisation method, which is based on the fact that a polarised neutron beam experiences rotation of the polarisation on its way through the sample because of the interaction with the internal magnetic field. Halpern and Holstein (1941) proposed exploiting this effect for the determination of the inner magnetisation of ferromagnetic materials. The first depolarisation experiments were made by Burgy *et al.* (1950) which gave information on the mean domain size. The capabilities of the method have been significantly increased by Rekveldt (1973, 1976) who introduced the three-dimensional depolarisation technique which allows also the determination of the mean direction cosines and the mean direction correlations. However, there is no model independent way to extract these quantities. The main difficulties are the correlations between different domains which are inevitably present because of Maxwell's law (Rosman and Rekveldt 1990; Lientschnig *et al.* 1996).

Recently a tomographic extension of the three-dimensional neutron depolarisation method was proposed (Hochhold *et al.* 1996*a*, 1996*b*) which opens up the possibility of visualising magnetic domains within bulk materials. Such investigations of

* Refereed paper based on a contribution to the International Workshop on Nuclear Methods in Magnetism, held in Canberra on 21–23 July 1997.

the domain structure within bulk materials are of great interest for the material sciences but no suitable method is available to date. The idea of the new method is quite similar to standard x-ray transmission tomography. However, the analysis of these experiments is mathematically much more involved because the observables are tensors and not scalars. In the absence of a known analytical solution it is even not clear what data are required to extract the magnetic field distribution uniquely. Therefore the question of retrieval has been investigated by numerical means. We developed numerical iteration procedures which yielded surprisingly good results in our previous work (Hochhold *et al.* 1996*a*, 1996*b*).

In this paper we focus on the important question whether neutron magnetic tomography can actually be implemented experimentally. Before giving the arguments on experimental details we present, in Section 2, the mathematical formulation of the problem and discuss the presently available numerical backprojection algorithms. Specifically, we will introduce a refined iterative procedure which accounts exactly for the non-Abelian properties of the depolarisation matrices. In Section 3 we discuss the experimental aspects of neutron magnetic tomography. Two set-ups, a standard one and one based on modern neutron optical devices, are discussed and estimates for the measurement times are given assuming that the experiments are performed at the high flux reactor at ILL in Grenoble. Our estimates clearly indicate that neutron magnetic tomography is indeed within experimental reach with modern technology. Finally, a summary and an outlook is given in Section 4.

2. Theory

(2a) Spin Rotation Formalism

The depolarisation of a neutron beam by transmission through a sample is theoretically well understood and can be described either by the quantum mechanical scattering approach (Maleev and Ruban 1972, 1976) or by the semiclassical spin rotation formalism (Rekveldt 1973, 1976; Rosman and Rekveldt 1990). For the analysis of neutron magnetic tomography we adopt the latter. Here we briefly sketch the most important relations and assumptions.

A neutron beam moving through a homogeneous magnetic field \mathbf{B} changes its polarisation \mathbf{P} according to the equation of motion

$$\frac{d\mathbf{P}}{dt} = \gamma \mathbf{P} \times \mathbf{B}, \quad (1)$$

where $\gamma = 1.883 \times 10^8$ rad/sT is the gyromagnetic factor of the neutron. In what follows we assume that the neutron is moving in the z -direction with velocity v and express the time dependence directly in terms of the coordinate $z = z_0 + vt$. Introducing a matrix notation, equation (1) can be written as

$$\frac{d\mathbf{P}(z)}{dz} = \mathcal{A}(z) \cdot \mathbf{P}(z), \quad (2)$$

where $\mathcal{A}(z)$ represents the external product and depends on the velocity v and on the components of the magnetic field $\mathbf{B} = (B_x, B_y, B_z)$ along the ray,

$$\mathcal{A} = \frac{\gamma}{v} \begin{pmatrix} 0 & B_z & -B_y \\ -B_z & 0 & B_x \\ B_y & -B_x & 0 \end{pmatrix}. \quad (3)$$

For a homogeneous magnetic field the solution of equation (2) yields a rotation of $\mathbf{P}(z)$ through the angle $\alpha = (\gamma/v)|\mathbf{B}|(z - z_0)$ with the rotation axis $\hat{\mathbf{n}} = \mathbf{B}/|\mathbf{B}|$, i.e.

$$\mathbf{P}(z) = \mathcal{D}(\hat{\mathbf{n}}, \alpha)\mathbf{P}(z_0). \quad (4)$$

Here, $\mathcal{D}(\hat{\mathbf{n}}, \alpha)$ is a rotation matrix.

A ferromagnetic material is characterised by the existence of magnetic domains which are separated by thin domain walls. In the neutron depolarisation method it is well established that the effect of the domain walls on \mathbf{P} is negligible and therefore it is justified to apply equation (1) along the whole beam line. This leads to the formal solution,

$$\mathcal{D} = \exp \left(\int_{z_0}^{z_e} dz \mathcal{A}(z) \right), \quad (5)$$

where z_0 is the entrance point of the beam into the sample and z_e is the exit point. The arrow on the integral indicates the path ordering and accounts for the non-Abelian properties of \mathcal{A} .

So far we have considered infinitely thin beams and therefore the matrix \mathcal{D} of equation (5) is still a pure rotation matrix leaving the length of the polarisation vector unchanged. In realistic depolarisation measurements the cross sections of the beam and the aperture of the detector exceed the typical size of domains. Therefore, one measures an average over an ensemble of infinitely thin beams and obtains a depolarisation matrix $\langle \mathcal{D} \rangle$ which includes also a reduction of the beam polarisation due to averaging. A typical set up for three-dimensional depolarisation measurements looks similar to that of Fig. 4 but with a fixed sample holder.

(2b) Tomographic Problem

The tomographic extension of the three-dimensional depolarisation method is straightforward and a sketch of the geometry is displayed in Fig. 1. Similar to standard x-ray transmission tomography one scans a specific plane of the sample by neutron beams of varying directions. For simplicity we assume that we can use infinitely thin neutron beams and obtain a set of rotation matrices \mathcal{D} .

The retrieval of the magnetic domain structure from tomographic neutron depolarisation data requires the solution of the inverse problem associated to equation (5). Formally it looks quite similar to the relations in x-ray transmission tomography but the new feature of path ordering increases the difficulties of its solution significantly.

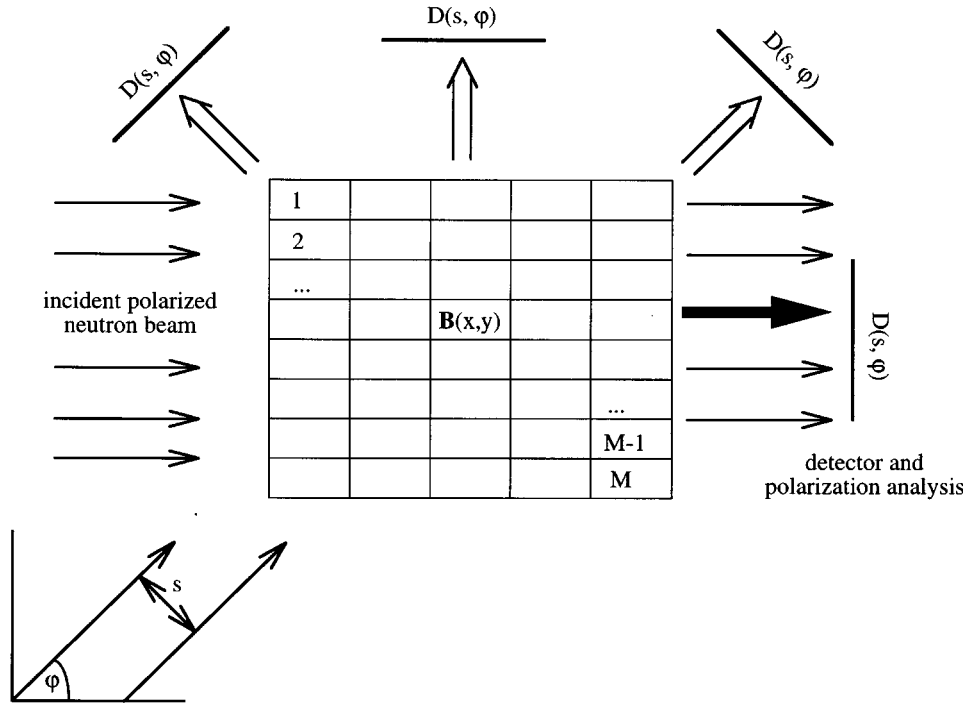


Fig. 1. Geometry of a tomographic neutron depolarisation measurement. The cross section under investigation is scanned by beams of different direction φ and lateral position s . For each beam line three-dimensional polarisation measurements are performed, which determine the 3×3 -matrix $\mathcal{D}(s, \varphi)$. The whole set of matrices $\mathcal{D}(s, \varphi)$ forms the input of the inversion algorithm.

In the absence of any analytic solution of this problem we have developed iterative numerical procedures of various accuracy in order to extract the magnetisation distribution from the set of measured \mathcal{D} -matrices. The basic ansatz of the procedures is the factorisation of \mathcal{D} ,

$$\mathcal{D} = \mathcal{L} \cdot \mathcal{K} , \quad (6)$$

where \mathcal{L} contains only pure line integrals and is defined by

$$\mathcal{L} = \exp \left(\int_{z_0}^{z_e} dz \mathcal{A}(z) \right) . \quad (7)$$

The correction matrix \mathcal{K} accounts for the path ordering and cannot be given by a simple algebraic expression. If we know \mathcal{L} for each ray the tomographic problem reduces to that of three independent scalar line integrals

$$\int_{z_0}^{z_e} dz B_k^{(1)}(z) = \frac{v}{\gamma} (\ln \mathcal{D})_{i,j} , \quad \text{with} \begin{pmatrix} k = x, & i, j = y, z \\ k = y, & i, j = z, x \\ k = z, & i, j = x, y \end{pmatrix} , \quad (8)$$

which can be inverted individually by standard Radon backtransformation techniques (Barrett and Swindell 1981). In the context of equation (6) backprojection of the tensorial tomographic problem mainly requires a proper determination or estimate of the correction matrix \mathcal{K} .

(2c) *Numerical Algorithm*

To perform the backprojection of the tomographic data numerically we divide the specific cross section of the sample into square pixels of equal size and assume that each pixel carries a homogeneous magnetic field. Considering a specific ray which traverses N pixels the matrix \mathcal{D} can be written as a path ordered product of pixel-matrices \mathcal{D}_i ,

$$\mathcal{D} = \mathcal{D}_N \cdot \mathcal{D}_{N-1} \cdot \dots \cdot \mathcal{D}_1. \quad (9)$$

The matrix \mathcal{D}_i describes the rotation of the neutron polarisation within the i th pixel and is determined by the pixel magnetisation expressed by the matrix \mathcal{A}_i and the length Δz_i of the ray in the pixel,

$$\mathcal{D}_i = \exp(\mathcal{A}_i \Delta z_i). \quad (10)$$

For this ray the corresponding matrix \mathcal{L} is simply given by

$$\mathcal{L} = \exp\left(\sum_{i=1}^N \mathcal{A}_i \Delta z_i\right). \quad (11)$$

Substituting equations (9)–(11) into equation (6) one can derive an expansion of \mathcal{K} in terms of commutators of \mathcal{A} -matrices of different pixels,

$$\mathcal{K} = \exp\left(\frac{1}{2} \sum_{j=1}^{N-1} [\mathcal{A}_{j+1} \Delta z_{j+1}, \sum_{k=1}^j \mathcal{A}_k \Delta z_k] + \dots\right). \quad (12)$$

This expansion, which is related to the Baker–Hausdorff–Campbell formula, has been used to formulate various iterative numerical procedures for the determination of \mathcal{K} .

Lowest order approximation. In the simplest case, neglecting all commutators, \mathcal{K} becomes unity and one has only to perform standard Radon backtransformations. This lowest order approximation, which ignores completely the path ordering, has led to surprisingly good reconstructions of magnetisation distributions \mathbf{B} from simulated depolarisation data (Hochhold *et al.* 1996a). The quality of reconstruction depends strongly on the pixel size; in particular, the method fails if the pixel size exceeds a critical value.

First order path ordering. For a known magnetisation distribution we can evaluate each term of the expansion of \mathcal{K} . Specifically in the first order

approximation we included the first commutator term of the expansion, equation (12), and obtained an estimate $\mathcal{K}_{(1)}$ of the correction matrix \mathcal{K} ,

$$\mathcal{K}_{(1)} = \prod_{j=1}^{N-1} \exp \left(\frac{1}{2} \left[\mathcal{A}_{j+1} \Delta z_{j+1}, \sum_{k=1}^j \mathcal{A}_k \Delta z_k \right] \right). \quad (13)$$

Using $\mathcal{K}_{(1)}$ one can define a corrected $\mathcal{L}_{(1)} = \mathcal{D} \cdot \mathcal{K}_{(1)}^{-1}$ which yields via the standard Radon backtransformation an improved magnetisation distribution. Thus one can formulate an iterative procedure at least partially taking into account the path ordering. As the starting point of this procedure we use the magnetisation distributions extracted via the lowest order approximation. In several schematic examples we find improved convergence and an improved reconstruction of the magnetisation distribution (Hochhold *et al.* 1996b).

Refined algorithm—full path ordering. Recently we implemented a refined algorithm which includes completely the path ordering. In principle one can extend the first order approach and evaluate all higher order terms of the expansion, equation (12), explicitly. However, this procedure is tedious and time consuming and one is always forced to truncate it at some level. Hence, we have chosen a completely numerical approach. For a given magnetisation distribution we can evaluate theoretically for each ray the matrices $\mathcal{D}_{(th)}$ and $\mathcal{L}_{(th)}$ and hence a theoretical correction matrix $\mathcal{K}_{(\infty)}$,

$$\mathcal{K}_{(\infty)} = (\mathcal{L}_{(th)})^{-1} \cdot \mathcal{D}_{(th)}. \quad (14)$$

Assuming that $\mathcal{K}_{(\infty)}$ is also a good approximation in the case of a slightly different magnetisation distribution, we can apply $\mathcal{K}_{(\infty)}$ to the experimental depolarisation matrix \mathcal{D} , thus obtaining a corrected operator

$$\mathcal{L}_1 = \mathcal{D} \cdot (\mathcal{K}_{(\infty)})^{-1}. \quad (15)$$

Because of the exponential functions involved, both $\mathcal{L}_{(th)}$ and $\mathcal{K}_{(\infty)}$ are invertible and equations (14) and (15) can always be evaluated. Applying the standard Radon backtransformation to the set of \mathcal{L}_1 matrices one obtains the associated magnetisation distribution which can be used again to calculate new matrices $\mathcal{D}_{(th)}$ and $\mathcal{L}_{(th)}$. Thus one obtains an iterative procedure which completely includes the path ordering and should yield in the case of convergence the exact magnetisation distribution.

We have implemented this algorithm numerically and checked its reconstructive power analysing simulated neutron depolarisation data associated with a known magnetic field distribution. We consider the cross section of a specimen divided into 20×20 pixels, each one with a randomly oriented magnetisation $\mathbf{B}_i = B_S \cdot (n_x^i, n_y^i, n_z^i)$, characterised by the direction cosines n_j^i , $j = x, y, z$. In the simulations we restricted ourselves to square pixels of equal size and saturation magnetisation B_S . The plane considered was scanned by 854 neutron beams with a neutron velocity $v = 2000 \text{ m s}^{-1}$.

Following the procedure discussed previously we have reconstructed the magnetisation distribution using the lowest order approximation as a starting point. In order to judge the quality of reconstruction we introduce the mean deviation

$$\Delta = \frac{1}{M} \sum_{i,j} \left| n_{j,O}^i - n_{j,I}^i \right|, \quad (16)$$

where M is the number of pixels and the indices O and I refer to the direction cosines of the original and the image. In Fig. 2 the rate of convergence is displayed for two pixel sizes. The values $\Delta = 10^{-5}$ correspond to perfect agreement within numerical accuracy and are two to three orders of magnitude smaller than those achieved in the lowest order approach. It is obvious that in all cases considered the refined algorithm leads to a significant improvement of the reconstruction. The accuracy reached is within the numerical errors and represents a perfect reconstruction.

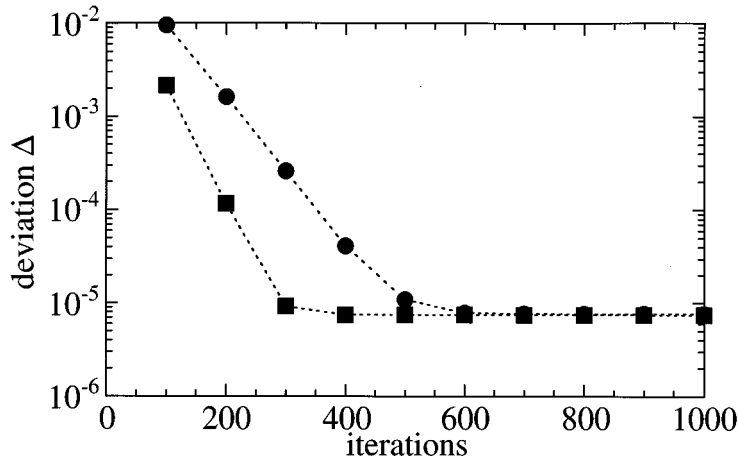


Fig. 2. Convergence of the refined iteration procedures for different pixel sizes, $0.8 \times 0.8 \mu\text{m}^2$ (circles) and $1.2 \times 1.2 \mu\text{m}^2$ (squares).

Since we find the solution by iteration the question of convergence of the procedure is essential. At present, convergence has always been achieved for pixel sizes up to $1.6 \times 1.6 \mu\text{m}^2$. The alignment of the magnetisation of several pixels to form magnetic domains of greater extension does not lead to a significant change of this behaviour. This can be concluded from our successful tests which included domains with sizes up to $9 \times 9 \mu\text{m}^2$. The failure of convergence for larger pixel sizes is due to the large rotation angle experienced by the polarisation vector in a single pixel. Hence the non-Abelian contributions dominate the path-ordered line integrals and do not allow the application of a perturbative approach. As a consequence the starting values of the iteration procedure (generated by the lowest order approach) do not exhibit the basic structures and are out of the range of the convergence. To improve on this a better method for the generation of the starting values is required if one wants to handle larger pixel sizes.

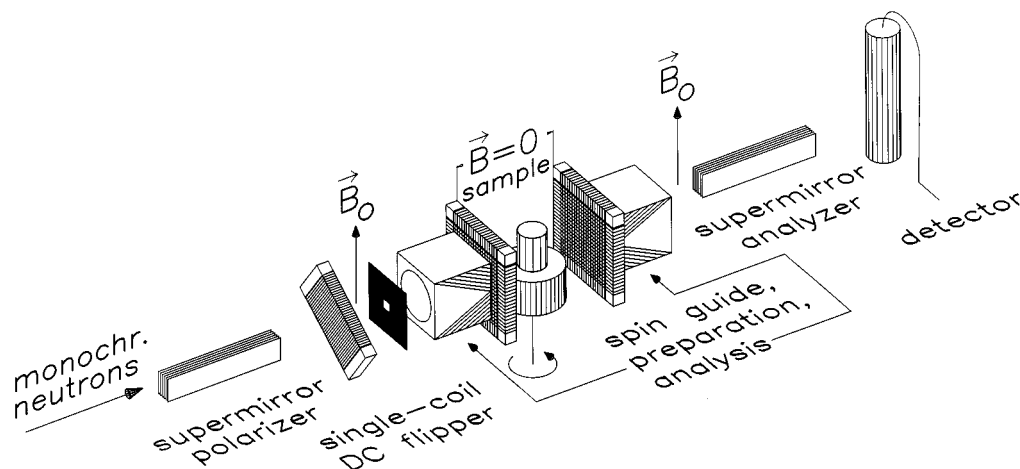


Fig. 3. Experimental set up for neutron magnetic tomography. The arrangement is in principle the same as for three-dimensional depolarisation measurements, except for the sample holder which must allow rotations and shifts of the sample with respect to the beam.

3. Experimental Feasibility

(3a) Parallel Beam Method

The experimental set up that is necessary to perform tensorial neutron magnetic tomography is in principle similar to three-dimensional neutron depolarisation facilities which are routinely used for domain structure studies of magnetic substances (Rekvelde 1973). However, the actual implementation of this novel technique depends crucially on the availability of a sufficiently high neutron flux. Therefore it is meaningful to install such a set up, which is shown schematically in Fig. 3, at a high flux neutron source such as the one at the Institute Laue–Langevin (ILL) in Grenoble. To obtain a realistic estimate of the time needed to perform a tomographic determination of the magnetic structure within a layer of the sample we use the well-known parameters of the three-dimensional neutron depolarisation instrument which is installed at the 250 kW TRIGA reactor of our university in Vienna. In this set up the incident neutron beam is monochromatised by Bragg reflection at a pyrolytic graphite single crystal and polarised parallel to a static magnetic guide field \mathbf{B}_0 by a Co–Ti supermirror assembly. The degree of polarisation of the transmitted beam is very high (about 99%). Activation of a DC spin flip coil allows inversion of the orientation of the polarisation relative to the field direction. The sample under investigation is placed in a field-free region between two spin turn coil systems which by controlled Larmor spin rotation allow orientation of the incident polarisation \mathbf{P}_i successively in all three directions of space and to project any component of the final polarisation vector \mathbf{P}_f onto the analysing direction of a second supermirror. By this procedure one can measure successively all nine elements of the depolarisation matrix \mathcal{D} which connects the incident and the final polarisation vector via $\mathbf{P}_f = \mathcal{D}\mathbf{P}_i$. Confining the beam to a small diameter and rotating the sample about a vertical axis in principle allows one to determine the depolarisation matrices for a large number of sample orientations, thereby yielding the set of data which is required for

tomographic reconstruction of the field distribution within the transmitted region of the sample. Insertion of a Cd diaphragm of 0.3 mm width and 20 mm height immediately behind the central mirror of the polariser assembly at 1.6 Å wavelength, a neutron intensity of $1.4 \times 10^3 \text{ s}^{-1}$ is found at the sample position. The scaling factor between the neutron flux of our TRIGA reactor in Vienna and that of the best existing neutron source, namely the high-flux reactor of the Institute Laue–Langevin (ILL) in Grenoble, is almost exactly 10^{-3} , which means that there the corresponding intensity would be of the order of $1.4 \times 10^6 \text{ s}^{-1}$.

To begin with, let us assume a beam diameter of 10 μm . At the ILL reactor the expected intensity at the sample position for such a small beam area would then be about 23 s^{-1} . The usual number of neutron counts to determine one of the nine matrix elements of the depolarisation matrix with reasonable statistical precision is of the order of 10^3 . Hence, under the realistic assumption that at least 40% of the intensity that traverses the sample is transmitted by the analysing mirrors, a total measurement time of typically 400 hours would be required to accumulate the depolarisation matrices of, say, 1500 different trajectories through the sample by this *conventional* parallel beam method of neutron magnetic tomography. At first glance this is quite a lot of time. But it is not hopelessly out of reach, and it could be realised in a straightforward manner by existing techniques and presently available neutron sources. There are, however, some possibilities to reduce the required measuring times drastically by almost two orders of magnitude, as we will discuss in the following sections.

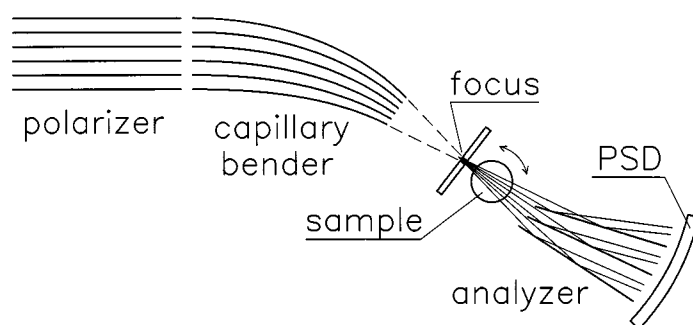


Fig. 4. Scheme of the divergent beam neutron magnetic tomography method. For the sake of clarity the spin manipulation components have been omitted. The individual neutron trajectories are resolved by a position sensitive detector (PSD). As indicated, polarisation analysis is performed by means of a stacked ensemble of supermirrors. For an alternative method of spin analysis see text.

(3b) Divergent Beam Method

Quite recently novel multifibre neutron optical devices have been developed which consist of large arrays of curved polycapillary fibres, typically 10 μm in diameter (Kumakhov and Komarov 1990). These commercially available polycapillary optics allow one to guide thermal and cold neutrons by means of multiple total external reflections efficiently through very small radii of curvature ($\sim 1 \text{ m}$) and thus can fulfil many beam control functions including focussing, bending, collimating and splitting. For example, focussing of a large area neutron

beam ($50 \times 45 \text{ mm}^2$) to a spot width of about 0.5 mm FWHM which produces an average intensity gain of more than 80 at the focal spot has been reported (Xiao *et al.* 1994). Even higher intensity enhancement factors (~ 100) and smaller spot sizes ($150 \mu\text{m}$) have been achieved with monolithic polycapillary lenses (Chen-Mayer *et al.* 1996). However, this improvement is obtained with reduced primary beam diameters ($\sim 4 \text{ mm}$).

Such appealing focusing devices could be used to realise a highly efficient neutron magnetic tomography facility as shown in Fig. 4. One has to take into account that focusing causes the beam to be divergent behind the focal plane, with a typical divergence angle of 20° . Using a high resolution imaging detector, which for our purpose could either be a video radiation detector (VRD) (Downing *et al.* 1993) or a position-sensitive Si-strip detector with Gd-foil converter (Bruckner and Rauch 1996; Bruckner *et al.* 1996), placed behind an analysing array of supermirrors should allow one to detect most of the neutrons that pass through the focal plane diaphragm and traverse the sample as divergent rays.

There is some degree of freedom with respect to the type of polarisation analyser used. Instead of the stacked ensemble of supermirrors in Fig. 4 (which by the way would allow some ingenious additional focusing/defocusing concepts), the recently developed spin-polarised ^3He absorption filters might likewise be chosen (Surkan *et al.* 1997). Such novel devices might lead to an even more efficient exploitation of the available neutron flux. If we assume an intensity gain of only 40, which is just 50% of what has already been achieved, this *divergent beam method* could reduce the total measuring time for a complete set of tomographic data to about 10 hours.

(3c) Neutron Interferometric Phase Contrast Tomography

Polarised neutron interferometry (Badurek 1996) in principle offers the interesting possibility of implementing a neutron magnetic tomography experiment which does not require the use of thin beams. It is based on the phase contrast

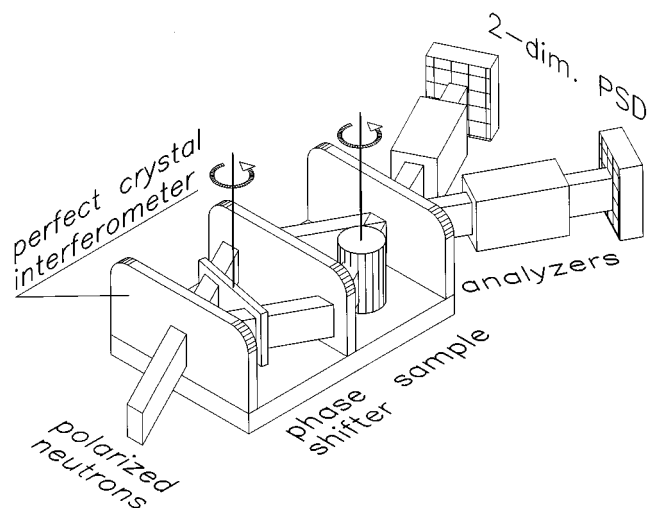


Fig. 5. Set up used for neutron interferometric phase contrast tomography.

topography method introduced by Schlenker and Baruchel (1986). Rauch and Seidl (1987) have shown that the interference contrast depends on the size of magnetic domains of the sample inserted in one arm of the interferometer.

Consider a situation where in one arm of a Mach-Zender-type perfect crystal neutron interferometer a magnetic sample is inserted, as indicated in Fig. 5. Due to the coherence properties of the two interfering partial beams there is a one-to-one correspondence of the incident and the emerging rays even for a large beam cross section. Upon passage through a series of N successive magnetic domains the neutron wavefunction is modified by the spin rotation operator

$$U = \prod_{j=1}^N \exp(-i\boldsymbol{\sigma} \cdot \boldsymbol{\alpha}_j/2), \quad (17)$$

where the spin rotation vectors $\boldsymbol{\alpha}_j = \alpha_j \hat{\boldsymbol{\alpha}}_j$ carry the information about the size of the j th domain and the magnitude and the orientation of its spontaneous magnetic induction. It can be shown that due to the noncommuting properties of the Pauli spin operator $\boldsymbol{\sigma}$ the phase shift of the neutron wavefunction under the action of the operator U has both a dynamical and a geometric component (Wagh *et al.* 1997).

A detailed theoretical treatment of this polarised neutron tomographic interference technique is in progress and will be published in a forthcoming paper. The phase information obtained from the tomographic measurement is directly related to the same line integrals along the neutron trajectories as discussed in the previous sections. Thus the domain structure of the sample could be reconstructed provided the magnetic phase shift distributions have been mapped for a sufficiently large number of sample orientations by means of position sensitive detectors placed behind a polarisation analyser. Using polarised neutrons in combination with full polarisation analysis implies a natural separation of nuclear and magnetic phase shift contributions.

4. Conclusions

In this paper we gave a comprehensive review of the theoretical and experimental aspects of neutron magnetic tomography. We outlined the basic formalism and presented the available numerical algorithms for the reconstruction of the distribution of the inner magnetic fields. In particular we outlined a refined iterative procedure which fully takes into account the path ordering. It is found by application to simulated data that this refined algorithm yields, within numerical accuracy, a perfect reproduction of the magnetic field distribution as long as the pixel sizes do not exceed a certain value. This result indicates that neutron magnetic tomography data would allow, at least from the mathematical point of view, extraction of the magnetic structure within bulk materials.

The accuracy and large quantity of data required for the experimental implementation of neutron magnetic tomography presents a very challenging task. We showed that standard measurements techniques cannot resolve typical domain sizes ($10 \times 10 \mu\text{m}^2$) in reasonable measuring times even with the highest available flux. The use of recently developed neutron optical devices in a dedicated device for neutron magnetic tomography would enable an experimental implementation of the technique.

At the moment it is the main theoretical goal to increase the capabilities of the method of analysis towards larger pixel sizes. Here, the main difficulties stem from the poor starting values as well as from the ambiguity arising from the logarithm occurring in equation (8). Both problems are under consideration and significant improvements can be expected in the near future.

Further progress is also expected from the experimental side. The recent development of broadband absorption neutron spin filters (NSF) which use compressed, polarised ^3He gas (Surkan *et al.* 1997) might strongly enhance the experimental feasibility of neutron magnetic tomography for two reasons:

(i) NSF just absorbs one neutron spin state but unlike reflecting mirrors it does not change the spatial distribution of the transmitted spin state.

(ii) It also allows one to polarise and to analyse neutrons with wavelengths smaller than 0.1 nm. The use of faster neutrons leads to reduced rotations of the polarisation vector per pixel and hence the range of convergence of the inversion algorithms is extended to larger pixel sizes.

In summary, neutron magnetic tomography is indeed a promising technique for the visualisation of magnetic domains in bulk materials. The proposed development of neutron interferometric phase contrast tomography is very appealing because of the well known accuracy of interferometric measurements. Theoretical and experimental investigations of this topic are in progress.

Acknowledgments

This work has been supported by Fonds zur Förderung der wissenschaftlichen Forschung in Österreich, project No. P10969-PHY.

References

- Badurek, G. (1996). *J. Phys. Soc. Jpn Suppl.* **65**, 60.
- Barrett, H. H., and Swindell, W. (1981). 'Radiological Imaging' (Academic: New York).
- Bruckner, G., and Rauch, H. (1996). *J. Neutron Res.* **4**, 141.
- Bruckner, G., Rauch, H., Rudge, A., Weilhammer, P., and Dulinski, W. (1996). *Proc. SPIE* **2876**, 554.
- Burgy, M., Hughes, D. J., Wallace, J. R., Heller, R. B., and Woolf, W. E. (1950). *Phys. Rev.* **80**, 953.
- Chen-Mayer, H. H., Mildner, D. R. F., Sharov, V. A., Ullrich, J. B., Ponomarev, I. Yu., and Downing, R. G. (1996). *J. Phys. Soc. Jpn Suppl.* **65**, 319.
- Downing, R. G., Zeissler, C. J., and Chen, H. (1993). *SPIE Conf. Proc.* **1737**, 308.
- Halpern, O., and Holstein, T. (1941). *Phys. Rev.* **59**, 960.
- Hochhold, M., Leeb, H., and Badurek, G. (1996a). *J. Magn. Magn. Mater.* **157/58**, 575.
- Hochhold, M., Leeb, H., and Badurek, G. (1996b). *J. Phys. Soc. Jpn Suppl.* **65**, 292.
- Kumakhov, M. A., and Komarov, F. F. (1990). *Phys. Rep.* **191**, 289.
- Lientschnig, G., Leeb, H., and Badurek, G. (1996). *J. Magn. Magn. Mater.* **157/58**, 316.
- Maleev, S. V., and Ruban, V. A. (1972). *Sov. Phys. JETP* **35**, 222.
- Maleev, S. V., and Ruban, V. A. (1976). *Sov. Phys. Solid State* **18**, 1331.
- Rauch, H., and Seidl, E. (1987). *Nucl. Instrum. Methods A* **255**, 32.
- Rekveltdt, M. Th. (1973). *Z. Phys.* **259**, 391.
- Rekveltdt, M. Th. (1976). *J. Magn. Magn. Mater.* **1**, 342.
- Rosman, R., and Rekveltdt, M. Th. (1990). *Z. Phys. B* **79**, 61.
- Schlenker, M., and Baruchel, J. (1986). *Physica B* **137**, 309.
- Surkan, R., Becker, J., Ebert, M., Grossmann, T., Heil, W., Hofmann, D., Humblot, M., Leduc, M., Otten, E. W., Rohe, D., Siemensmeyer, K., Steiner, M., Tasset, F., and Trautmann, N. (1997). *Phys. Rev. A* **384**, 444.

- Wagh, A. G., Rakhecha, V. C., Summhammer, J., Badurek, G., Weinfurter, H., Allman, B. E., Kaiser, H., Hamacher, K., Jacobson, D. L., and Werner, S. A. (1997). *Phys. Rev. Lett.* **78**, 755.
- Xiao, Q. F., Sharov, V. A., Mildner, D. R. F., Downing, R. G., Gao, N., and Gibson, D. M. (1994). *Rev. Sci. Instrum.* **65**, 3399.

Manuscript received 23 July 1997, accepted 7 January 1998